Thin Solid Films 642 (2017) 20–24

Contents lists available at ScienceDirect

Thin Solid Films

journal homepage: www.elsevier.com/locate/tsf

Approach to form planar structures based on epitaxial $Fe_{1-x}Si_x$ films grown on Si(111)

A.S. Tarasov[a,b], A.V. Lukyanenko[a,b,*], I.A. Tarasov[a], I.A. Bondarev[a,b], T.E. Smolyarova[a,b], N.N. Kosyrev[a], V.A. Komarov[a,b], I.A. Yakovlev[a], M.N. Volochaev[a,c], L.A. Solovyov[d], A.A. Shemukhin[e], S.N. Varnakov[a], S.G. Ovchinnikov[a,b], G.S. Patrin[a,b], N.V. Volkov[a]

[a] Kirensky Institute of Physics, Federal Research Center KSC SB RAS, Krasnoyarsk 660036, Russia
[b] Institute of Engineering Physics and Radio Electronics, Siberian Federal University, Krasnoyarsk 660041, Russia
[c] Siberian State Aerospace University, Krasnoyarsk 660014, Russia
[d] Institute of Chemistry and Chemical Technology, Federal Research Center KSC SB RAS, 660036 Krasnoyarsk, Russia
[e] M.V.Lomonosov Moscow State University, Skobeltsyn Institute of Nuclear Physics, Moscow 119991, Russia

ARTICLE INFO

Keywords:
Iron silicides
Wet etching
Planar structures
MOKE microscopy

ABSTRACT

An approach to form planar structures based on ferromagnetic $Fe_{1-x}Si_x$ films is presented. Epitaxial $Fe_{1-x}Si_x$ iron-silicon alloy films with different silicon content (x = 0–0.4) were grown on Si(111) substrates. Structural in situ and ex situ characterization of the films obtained was made by X-ray diffraction, reflective high-energy electron diffraction, Rutherford backscattering spectrometry and transmission electron microscopy, which confirmed single crystallinity and interface abruptness for all films. Etching rates in the wet etchant (HF: HNO_3: H_2O = 1: 2: 400) for the films with various chemical composition were obtained. A nonmonotonic dependence of the etching rate on silicon content with a maximum for the composition $Fe_{0.92}Si_{0.08}$ was discovered. Moreover, the etching process is vertical and selective in the etching solution, i.e., the etching process takes place only in silicide film and does not affect substrate. As an example, a four-terminal planar structure was made of $Fe_{0.75}Si_{0.25}$/Si(111) structure using the etching rate obtained for this silicon content. Magneto-optical Kerr effect (MOKE) microscopy and transport properties characterization indicated successful etching process.

1. Introduction

At present, iron silicides are under intensive research in connection with their prospective use in different fields of electronics. Semiconducting iron silicide β-$FeSi_2$ attracts attention due to its potential application as a material for light emitting diodes and as a thermoelectric material [1,2]. Moreover, a direct band gap observed of 0.87 eV [3,4,5] and large optical absorption coefficient ($\alpha > 10^5\ cm^{-1}$) are favorable for photovoltaic utilization. Silicides with higher iron content, particularly Fe_3Si phase, is the most interesting for spintronics application. The Fe_3Si silicide has a relatively high Curie temperature of approximately 840 °C and a high degree of spin polarization of conduction electrons [6]. Besides, Fe_3Si lattice parameter of 0.564 nm [7] allows for performing epitaxial growth on semiconductor substrates of GaAs [8], Ge [9], Si [10,11] and on dielectric MgO(001) substrates [12] or on a several-nanometer-thick MgO tunneling barrier on GaAs(001) [13], which can improve spin injection efficiency into semiconductor. Moreover, the magnetic and electronic properties of such iron-rich epitaxial $Fe_{1-x}Si_x$ thin films (x = 0–0.4) can be tuned by varying the chemical order [14,15]. In these crystalline systems, three different bcc-like structures (D03, B2, A2), each with a different degree of chemical order, are possible. The A2 structure is a chemically disordered random bcc solid solution, and the B2 structure is a partially ordered CsCl structure with Fe on the cube corner sites, and Fe/Si randomly arranged on the body center sites. Finally, the D03 structure is chemically ordered with Fe on the cube corners and Fe and Si alternating in the body centers [16]. In particular, increasing silicon content leads to a decrease in the carrier concentration, which is important in the context of the resistivity mismatch in spin transistors devices without an oxide tunnel barrier [17]. Moreover, this can also bring about a larger magneto-optical Kerr effect than in case of bcc- Fe, that is crucial for magnetophotonic applications [18]. Thus, compatibility with semiconductor technology, non-toxicity, and abundance in the Earth's crust make iron-silicon alloy films an attractive candidate for many uses in electronics. It is clear that creation of various functional electronic and photonics devices implies a formation of different

* Corresponding author at: Kirensky Institute of Physics, Federal Research Center KSC SB RAS, Krasnoyarsk 660036, Russia.
E-mail address: lav@iph.krasn.ru (A.V. Lukyanenko).

http://dx.doi.org/10.1016/j.tsf.2017.09.025
Received 14 February 2017; Received in revised form 15 August 2017; Accepted 12 September 2017
Available online 14 September 2017
0040-6090/ © 2017 Elsevier B.V. All rights reserved.

silicide layer topologies and requires controlled etching of the films with different silicon content. However, the question of wet chemical etching rates of the epitaxial $Fe_{1-x}Si_x$ alloy films has not been enlightened enough in the literature available [19].

In this work, we present an easy way to fabricate planar multi-terminal structures based on epitaxial thin films $Fe_{1-x}Si_x$/Si(111) with different silicon content ($0 < x < 0.4$) by photolithography and wet chemical etching. Structural, magneto-optical and transport properties are presented for characterization and control of test four-terminal $Fe_{0.75}Si_{0.25}$/Si(111) planar structure fabrication.

2. Experiment

The $Fe_{1-x}Si_x$ films were formed on 1°- miscut vicinal *n*-doped Si (111) substrate ($\rho = 7.5\ \Omega$ cm) at 400 K by molecular beam epitaxy (MBE) in ultrahigh vacuum conditions (UHV) [20]. Details of the epitaxial iron silicide synthesis technology with the DO3 structure were described previously [10]. Different chemical composition of the $Fe_{1-x}Si_x$ alloy films ($0 < x < 0.4$) was achieved through co-deposition of iron and silicon by varying Fe and Si flow ratio. Thus, eight samples with different Si content were obtained ($0 < x < 0.4$). Correspondence of the sample number is listed below in Table 1. Epitaxial film growth was controlled in situ by reflection high-energy electron diffraction (RHEED) and ex situ X-ray diffraction (XRD) analysis. In addition, the structural properties of the films were investigated by transmission electron microscopy (TEM) and atomic force microscopy (AFM). The crystallinity of the layers grown was quantitatively investigated using Rutherford backscattering spectrometry (RBS) channeling measurements. The chemical composition of the samples was verified by both RBS and XRD methods. To form a multi-terminal planar structure – conventional photolithography and wet chemical etching with constant agitation and temperature of 22 °C in a liquid mixture of hydrofluoric acid and nitric acid (HF: HNO_3: H_2O = 1: 2: 400 at 22 °C) [19] were utilized. Control of the etching process was performed using atomic force microscopy (AFM) and magneto-optical Kerr effect (MOKE) microscopy with the help of NanoMOKE 2 installation. Test transport properties measurements of $Fe_{0.75}Si_{0.25}$ film and $Fe_{0.75}Si_{0.25}$-based planar structure were performed at cryogenic probe station Lakeshore EMPX-HF 2 and home built facility [21] equipped with a helium cryostat and KEITHLEY-2634 current/voltage source meter in the temperature range from 4.2 K to 300 K.

3. Results and discussions

X-ray diffraction (XRD) analysis was performed on a PANalytical X'Pert PRO diffractometer equipped with a solid state detector PIXcel on Cu Ka radiation. The in-plane epitaxial orientation was analyzed using asymmetrical φ-scans of reflections {224} from the $Fe_{1-x}Si_x$ alloy films and Si-substrate. Typical φ-scan for the sample No. 3 (Fig. 1b) reveals the following orientation relationship: $Fe_{0.75}Si_{0.25}$

Table 1
Parameters of the epitaxial $Fe_{1-x}Si_x$ films.

No. sample number	Chemical composition (according to XRD)		Thickness, Å	Etching rate υ, Å/s	Average roughness of as-grown film R_a(nm)
	Fe, at.%	Si, at.%			
1	60	40	700	1.8	1.24
2	67.2	32.8	524	9.1	1.45
3	74.7	25.3	686	51.8	1.13
4	82.7	17.3	1000	88.0	2.19
5	85.1	15.9	967	95.1	2.46
6	92	8	884	170.6	2.35
7	96.8	3.2	1008	152.7	2.30
8	100	0	250	52.6	1.17

(111) [1–21]||Si(111) [11–2] and shows no twinning. An appearance of a double peak on φ-scan for reflections {224} from the substrate is due to the splitting of $K\alpha_{1,2}$. For one of the peaks, $K\alpha_2$ is not visible because due to the fact that the substrate surface Si(111) has a miscut angle of 1° and as a result diffraction angle changes during the rotation. For the crystal structure analysis, a series of characteristic reflections 111, 222, 333 and 444 from the $Fe_{0.75}Si_{0.25}$ film (sample No. 3) were measured (Fig. 1(a)). An additional tilt of 1° was applied to reduce the Si(111) reflection. The cubic (Fm3m) lattice parameter a = 5.666(1) Å was determined from the XRD pattern by the derivative difference minimization method [22]. The silicon content of the $Fe_{1-x}Si_x$ alloy films was obtained by estimation of specific volume for one silicon atom in the $Fe_{1-x}Si_x$ unit cell. Crystal quality and chemical composition of the epitaxial $Fe_{1-x}Si_x$ alloy films were studied with the RBS method in combination with the channeling on accelerator HVEE AN-2500 (analytical equipment of M.V. Lomonosov Moscow State University, Skobeltsyn Institute of Nuclear Physics). Analyzing energy beam of helium ions He^+ was 1.8 MeV at a scattering angle of 165° relative to the direction of propagation of the beam. Each sample was studied in two modes: the beam incident is parallel to the crystallographic axis 〈111〉 direction and parallel to the direction not containing open channels, i.e., oblique 〈111〉 direction. The 〈111〉 direction in the crystal was determined according to a measurement of output backscattering ions in the sample dependent on a change of beam angle incidence. Typical RBS spectra for $Fe_{1-x}Si_x$ alloy films (sample No. 3) are shown in Fig.2(b). The minimum yield of backscattered He ions χ_{min} of 19.5% was obtained for $Fe_{0.75}Si_{0.25}$ alloy film from the ratio of the amplitude of Fe signal for the channeling spectrum to that for the random spectrum. The value obtained is comparable to the χ_{min} reported earlier by Y. Maeda et al. [23] and approximately two times lower than the value achieved in work [24], which indicates high crystal quality of the film. Thus, comparison of the data on the chemical composition of the $Fe_{1-x}Si_x$ alloy films obtained by both XRD and RBS methods indicates their good agreement (Fig. 2). Chemical composition values of the $Fe_{1-x}Si_x$ are listed in Table 1. Since the results obtained by XRD method are more representative than those one obtained by the RBS method, we chose them for further use in the article. Thus, X-ray irradiation examines a bigger area of the samples in comparison to the case of RBS method, where an analyzed area was about only 1 mm.

Cross-sections of the films obtained were prepared using a focused ion beam (FIB) FB-2100 (Hitachi, Japan) installation for electron microscopic investigations. Typical TEM images along the zone axis [110] for two $Fe_{1-x}Si_x$ alloy (x = 0.25, 0.17) compounds are shown in Fig. 3 (a) and Fig. 3 (b). As can be seen from the figure the films are uniform and do not contain differently oriented grains, a roughness of the film surface is about 2–3 nm. Additionally, one can see the sharp and smooth interface between the film and substrate without interdiffusion layer, which indicates high crystal quality of the samples. Electron diffraction patterns showed on Fig. 3(c) and Fig. 3(d) demonstrate diffraction peaks from the iron silicide and silicon and confirm the result obtained by XRD. Typical surface morphology obtained by AFM is shown in Fig. 3(e). As-grown film roughness R_a rises from 0.5 nm for Si (111) substrate to 1–3 nm for the films with different silicon content (see Table 1), which confirms TEM results.

After the characterization, we moved to the etching process in order to create planar structure. The mask was coated using the standard photolithography method to perform further etching operation. Processing of the samples in nitric acid solution did not produce satisfactory results. The epitaxial $Fe_{1-x}Si_x$ alloy films with different x value did not etch equally well. The best etching uniformity is achieved when adding hydrofluoric acid. Film area coated with photoresist was protected from etching (acid) solution while the rest of the film was removed in a suitable solution of hydrofluoric acid and nitric acid HF: HNO_3: H_2O = 1: 2: 400 [19]. Surface treatment was carried out in the etching solution with constant agitation and temperature of 22 °C followed by washing in distilled water. Etching rate for each chemical

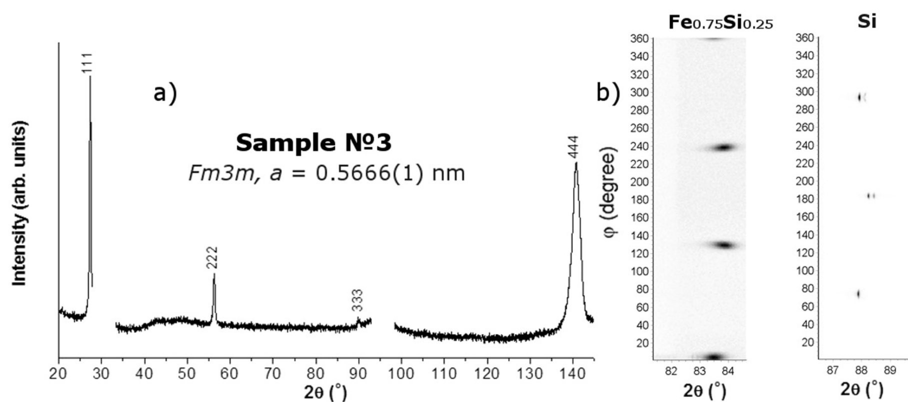

Fig. 1. Observed XRD patterns for four characteristic diffraction peaks of $Fe_{0.75}Si_{0.25}$ (a). 2D–images for φ-scans of reflections {224} from $Fe_{0.75}Si_{0.25}$ film and Si-substrate (b).

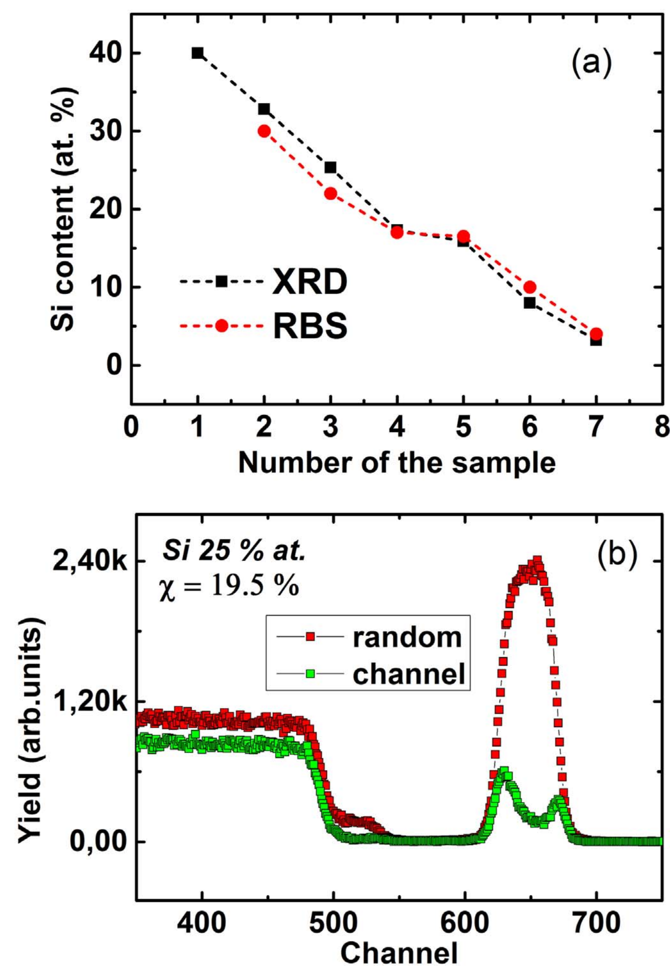

Fig. 2. Si content (at. %) obtained from XRD and RBS measurements (a). RBS spectra for $Fe_{0.75}Si_{0.25}$/Si(111) deposited at 400 K (b).

composition of the $Fe_{1-x}Si_x$ alloy films is given in Table 1. A non-monotonic dependence of the etching rate on silicon content was discovered. The rate rises with decreasing silicon content and reaches a maximum at $Fe_{0.92}Si_{0.08}$ composition then drops sharply. Thus, the solution utilized is the most effective for $Fe_{0.92}Si_{0.08}$ chemical composition and can be successfully applied to other compounds including pure iron. We assume that etching mechanism is similar to the etching process involving aqua regia, where the oxidative action of nitric acid is enhanced in the presence of hydrochloric acid. In our case, the hydrochloric acid was replaced to hydrofluoric one, which includes more active a fluorine ion (which, like chlorine, is an oxidizing agent). A presence of strong acids in the etching solution provides etching process. In turn, a large amount of water reduces a concentration of the reactants for precise and accurate etching.

In addition, to control the etching process a vertical etching profile and roughness of the boundary were measured by AFM after the film removal process. Main difficulties of the wet chemical etching are deviation of side walls etched out from the normal profile, etching wedge formation and dissolving of the material under a protective mask. In order to carry out AFM measurements, we used a super-shard cantilever (NSG30_SS, © TipsNano) with a tip curvature radius of < 5 nm. Taking into account the thickness of the film and applying the procedure for reconstructing the probe, we can conclude that the angles of the side walls do not exceed 3°. As seen in Fig. 4 etching occurs vertically, which provides high-quality structures. Moreover, we compared as-grown films roughness R_a with the roughness of completely etched area R_a^e and Si substrate after temperature treatment in UHV condition, R_a^{Si}. The R_a^e and R_a^{Si} are equal but lower than R_a, which suggests that films are completely etched and the etching process takes place only in silicide film and does not affect substrate. This solution is valid only for $Fe_{1-x}Si_x$ alloy films without etching silicon substrate. We also fabricated a multi-terminal planar structure based on $Fe_{0.75}Si_{0.25}$ film and carried out an additional experiment to confirm this assumption.

Four-terminal planar structure (Fig. 5) was made of the $Fe_{0.75}Si_{0.25}$/Si(111) sample using the etching rate obtained for the chemical composition given. Complementary verification of successful etching process was probed by MOKE microscopy. This technique is useful to

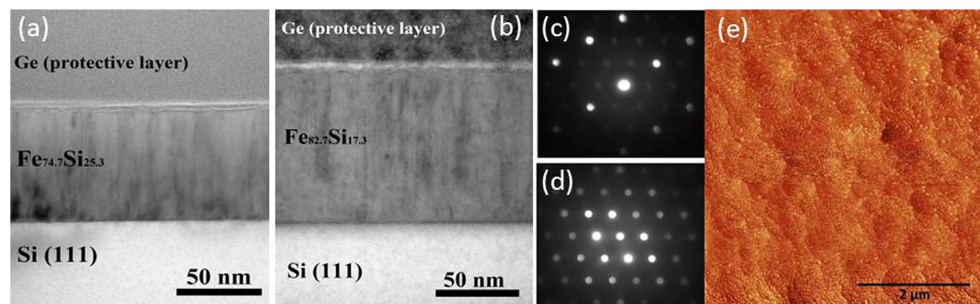

Fig. 3. Common structure properties of $Fe_{1-x}Si_x$ grown on Si (111). Cross-sectional TEM (a, b) images of two composition of $Fe_{1-x}Si_{1-x}$. The electron diffraction pattern of $Fe_{0.8}Si_{0.02}$ (c) and Si (d). The zone axis is parallel to [110] directions. Typical AFM image (e) of the sample surface.

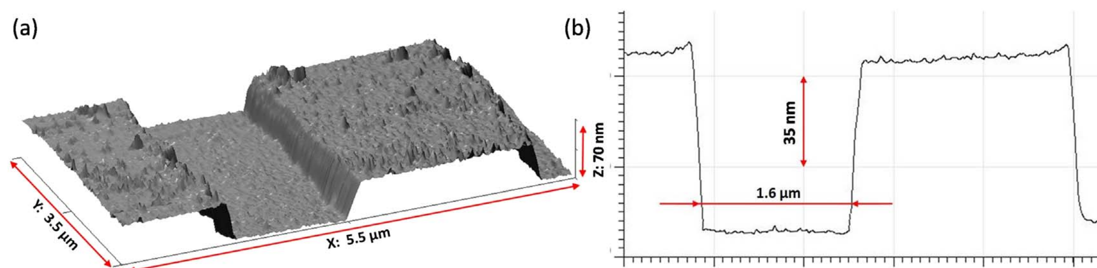

Fig. 4. AFM image (a) and 1-D profile (b) of device $Fe_{0.75}Si_{0.25}$/Si(111) etched.

determine whether a ferromagnetic material is left on the substrate after the etching. Fig. 5(a) shows a "magnetic map" of the planar structure indicating Kerr signal surface distribution in the magnetic field of 250 Oe with 3 µm resolution. Here one can see ferromagnetic electrodes, whose hysteresis loop is shown in the Fig. 5(b) (left axis), and diamagnetic silicon with linear magneto-optical signal (Fig. 5(b) (right axis)). This data confirms the $Fe_{0.75}Si_{0.25}$ film was completely etched in the area where the photoresist mask was absent, and only the electrodes are ferromagnetic. It should be noted, that probe laser spot diameter was about 5 µm, whereas map pixel was equal 3 µm. Therefore, during the scanning process of electrode edges, the probe laser spot fell on both $Fe_{0.75}Si_{0.25}$ and Si surfaces, which resulted in that a color gradient between the $Fe_{0.75}Si_{0.25}$ and Si areas are observed instead only two colors, which should be over the whole map. Nevertheless, MOKE signal from $Fe_{0.75}Si_{0.25}$ electrode surface is practically constant which proves (i) high film quality and (ii) high $Fe_{0.75}Si_{0.25}$ film protection by the mask during the etching.

One should take into account that below some thicknesses an iron-silicon alloy film can represent small separated islands on the silicon surface. Such $Fe_{0.75}Si_{0.25}$ islands are expected to be superparamagnetic, which requires a higher magnetic field to reach saturation magnetization than it was used for the MOKE mapping (250 Oe). Thus, as additional evidence of successful etching, the transport characteristic measurements of the $Fe_{0.75}Si_{0.25}$ films and $Fe_{0.75}Si_{0.25}$-based planar structure were carried out. In case if the film was not completely etched, a metallic-like behavior of the planar structure resistivity should be expected. Temperature dependence of the resistance of two samples is shown in Fig. 6. At investigated temperature region, the $Fe_{0.75}Si_{0.25}$ film resistance demonstrates a typical metallic behavior as expected. Besides, the resistivity value rises from 55 µOhm·cm at 4.2 K to 120 µOhm·cm at 300 K, which is comparable with other reported results [8,25]. One can easily see a knee (Fig. 6 black curve) observed around 250 K. It may be interpreted as current channel switching. Such phenomenon was found in different films like $Cu_{80}Co_{20}$ [26], Fe_3O_4 [27], Fe [28], LSMO [29] and other conductive films grown on Si substrate. The electrical current in structure measured with current in plane geometry shunt by Si bulk at high temperature, which depends on doping concentration and bias current. It can be explained as follows, if

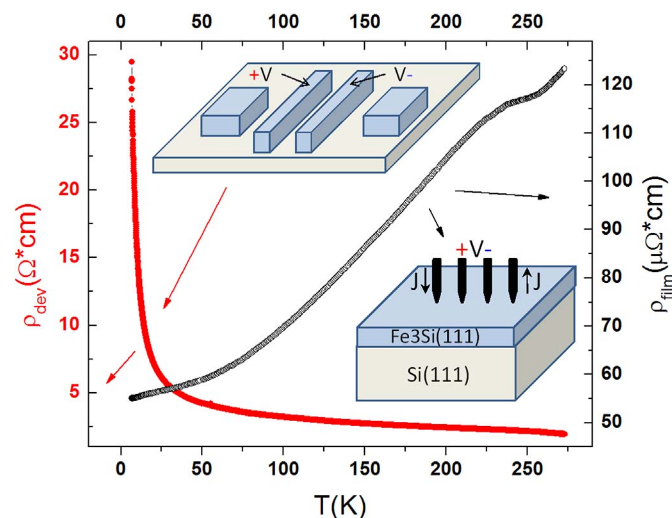

Fig. 6. Temperature dependences of the $Fe_{0.75}Si_{0.25}$ film resistance (right axis) and the $Fe_{0.75}Si_{0.25}$/Si(111) etched planar device (left axis). Insets show an experimental geometry for both samples.

substrate resistivity is relatively low, as in our case, part of electrons from metal film switch to silicon via thermionic emission process and current flows simultaneously in silicon and a conductive film. In equivalent circuit appears additional resistor in parallel mode. Consequently, the overall resistance drops. Conversely, the temperature dependence of the planar structure resistivity with 5 µm gap between electrodes is semiconducting. An exponential growth of resistivity with a decrease of the temperature is observed, which is due to impurity charge carrier freeze-out. Furthermore, the planar structure resistivity value at room temperature is greater by four orders of the magnitude comparing to the film. Thus, through the MOKE microscopy and the resistivity data, we can conclude that ferromagnetic and metallic $Fe_{0.75}Si_{0.25}$ compound was completely etched.

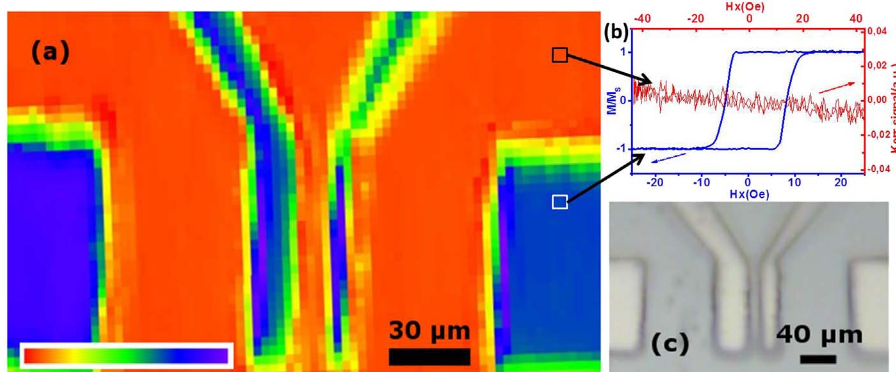

Fig. 5. Device surface distribution of the Kerr rotation angle in the magnetic field (a), $Fe_{0.75}Si_{0.25}$ MOKE hysteresis loop (b). Optical image of $Fe_{0.75}Si_{0.25}$/Si(111) 4-terminal planar device (c).

4. Conclusions

To conclude, we offer a simple and accessible approach for fabrication of multi-terminal planar structures based on ferromagnetic epitaxial $Fe_{1-x}Si_x$ alloy films on Si(111). This approach includes two stages, conventional photolithography, and wet chemical etching. Information on etching process and etching rates of the $Fe_{1-x}Si_x$ ($0 < x < 0.4$) alloy films in solution HF: HNO_3: H_2O = 1: 2: 400 along with their structural characteristics obtained in this work can be useful for researchers with interest in the science and technology of silicides and related materials. The approach described can be used for manufacturing of a necessary topology from a wide range of silicides for further application in optoelectronics, photonics, and spintronics.

Acknowledgment

We thank V.S. Zhigalov for assistance with the electron microscopy studies. The reported study was funded by Russian Foundation for Basic Research, Government of Krasnoyarsk Territory, Krasnoyarsk Region Science and Technology Support Fund to the research projects Nos. 16-42-243046, 16-42-242036 and 16-42-243060. The work was also supported by the Program of the President of the Russian Federation for the support of leading scientific schools (Scientific School 7559.2016.2).

References

[1] R. Amatya, R.J. Ram, Trend for thermoelectric materials and their earth abundance, J. Electron. Mater. 41 (2012) 1011–1019.
[2] E.G. Michel, Epitaxial iron silicides: geometry, electronic structure and applications, Appl. Surf. Sci. 117–118 (1997) 294–302.
[3] S.-W. Hung, P.-H. Yeh, L.-W. Chu, C.-D. Chen, L.-J. Chou, Y.-J. Wu, L.-J. Chen, Direct growth of β-FeSi2 nanowires with infrared emission, ferromagnetism at room temperature and high magnetoresistance via a spontaneous chemical reaction method, J. Mater. Chem. 21 (2011) 5704.
[4] D.Z. Chi, Semiconducting beta-phase FeSi2 for light emitting diode applications: recent developments, challenges, and solutions, Thin Solid Films 537 (2013) 1–22.
[5] Y.-H. Pai, K.-N. Cheng, G.-R. Lin, 1.55 μm photoluminescent iron silicide prepared by thermal diffusion of Iron nanoparticles into Si substrate, Communications and Photonics Conference and Exhibition (ACP), 2010, pp. 166–167.
[6] V.A. Niculescu, T.J. Burch, J.I. Budnick, A local environment description of hyperfine fields and atomic moments in$Fe_{3-x}T_x$Si alloys, J. Magn. Magn. Mater. 39 (1983) 223.
[7] M. Miya, K. Ueda, Yu-ichiro Ando, M. Kumano, T. Sadoh, K. Narumi, Y. Maedaet, Atomically controlled hetero-epitaxy of Fe3Si/SiGe for spintronics application, Thin Solid Films 517 (2008) 181–183.
[8] H. Vinzelberg, J. Schumann, D. Elefant, E. Arushanov, O.G. Schmidt, Transport and magnetic properties of Fe_3Si epitaxial films, J. Appl. Phys. 104 (2008) 093707.
[9] T. Sadoh, H. Kamizuru, A. Kenjo, M. Miyao, Atomically controlled molecular beam epitaxy of ferromagnetic silicide Fe_3Si on Ge, Appl. Phys. Lett. 89 (2006) 192114.
[10] I.A. Yakovlev, S.N. Varnakov, B.A. Belyaev, S.M. Zharkov, M.S. Molokeev, I.A. Tarasov, S.G. Ovchinnikov, Study of the structural and magnetic characteristics of epitaxial Fe3Si/Si(111) films, JETP Lett. 99 (2014) 527–530.
[11] K. Hamaya, K. Ueda, Y. Kishi, Y. Ando, T. Sadoh, M. Miyao, Epitaxial ferromagnetic Fe3Si/Si(111) structures with high-quality heterointerfaces, Appl. Phys. Lett. 93 (2008) 132117.
[12] Kh. Zakeri, I. Barsukov, N.K. Utochkina, F.M. Römer, J. Lindner, R. Meckenstock, U. von Hörsten, H. Wende, W. Keune, M. Farle, S.S. Kalarickal, K. Lenz, Z. Frait, Magnetic properties of epitaxial Fe_3Si/MgO(001) thin films, Phys. Rev. B 76 (2007) 214421.
[13] I. Barsukov, S. Mankovsky, A. Rubacheva, R. Meckenstock, D. Spoddig, J. Lindner, N. Melnichak, B. Krumme, S.I. Makarov, H. Wende, H. Ebert, M. Farle, Magnetocrystalline anisotropy and Gilbert damping in iron-rich $Fe_{1-x}Si_x$ thin films, Phys. Rev. B 84 (18) (2011) 180405.
[14] V.S. Zhandun, N.G. Zamkova, I.S. Sandalov, S.G. Ovchinnikov, Self-consistent mapping: effect of local environment on formation of magnetic moment in $\alpha-FeSi_2$, Phys. Rev. B 95 (2017) 054429.
[15] S. Yamada, J. Sagar, S. Honda, L. Lari, G. Takemoto, H. Itoh, A. Hirohata, K. Mibu, M. Miyao, K. Hamaya, Room-temperature structural ordering of a Heusler compound Fe_3Si, Phys. Rev. B 86 (2012) 174406.
[16] Julie Elizabeth, Tuning the Magnetic and Electronic Properties of FexSi Thin Films for Spintronics, Karel, UC Berkeley Electronic Theses and Dissertations, 2012.
[17] J. Karel, J. Juraszek, J. Minar, C. Bordel, K.H. Stone, Y.N. Zhang, J. Hu, R.Q. Wu, H. Ebert, J.B. Kortright, F. Hellman, Effect of chemical order on the magnetic and electronic properties of epitaxial off-stoichiometry $FexSi_{1-x}$ thin films, Phys. Rev. B 91 (2015) 144402.
[18] Y. Maeda, T. Ikeda, T. Ichikawa, T. Nakajima, B. Matsukura, T. Sadoh, M. Miyao, Magneto-optical properties of iron based Heusler alloy epitaxial films on Ge(111), Phys. Procedia 11 (2011) 200–203.
[19] T. Harianto, K. Sadakuni, H. Akinagal, T. Suemasu, Fabrication and current–voltage characteristics of Fe3Si/CaF2/Fe3Si magnetic tunnel junction, Jpn. J. Appl. Phys. 47 (8) (2008) 6310–6311.
[20] S.N. Varnakov, A.A. Lepeshev, S.G. Ovchinnikov, A.S. Parshin, M.M. Korshunov, P. Nevoral, Automation of technological equipment for obtaining multilayer structures in an ultrahigh vacuum, Instrum. Exp. Tech. 47 (2004) 839–843.
[21] N.V. Volkov, A.S. Tarasov, D.A. Smolyakov, A.O. Gustaitsev, V.V. Balashev, V.V. Korobtsov, The bias-controlled giant magnetoimpedance effect caused by the interface states in a metal-insulator-semiconductor structure with the Schottky barrier//Appl, Phys. Lett. 104 (2014) 222406.
[22] L.A. Solovyov, Full-profile refinement by derivative difference minimization, J. Appl. Crystallogr. 37 (2004) 743–749.
[23] Y. Maeda, Y. Kawakubo, Y. Noguchi, K. Narumi, S. Sakai, Ion beam analysis of Heusler alloy Fe3Si epitaxially grown on Si(111), Phys. Status Solidi C 11 (11–12) (2014) 1570–1573.
[24] K. Ueda, R. Kizuka, H. Takeuchi, A. Kenjo, T. Sadoh, M. Miyao, Influence of substrate orientation on low-temperature epitaxial growth of ferromagnetic silicide Fe3Si on Si, Thin Solid Films 515 (2007) 8250–8253.
[25] H.Y. Hung, S.Y. Huang, P. Chang, W.C. Lin, Y.C. Liu, S.F. Lee, M. Hong, J. Kwo, Strong crystal anisotropy of magneto-transport property in Fe3Si epitaxial film, J. Cryst. Growth 323 (2011) 372–375.
[26] J. Dai, L. Spinu, K.Y. Wang, L. Malkinski, J. Tang, Channel switching and magnetoresistance of a metal-SiO2-Si structure, J. Phys. D. Appl. Phys. 33 (2000) L65–L67.
[27] V.A. Vikulov, A.A. Dimitriev, V.V. Balashev, T.A. Pisarenko, V.V. Korobtsov, Low-temperature conducting channel switching in hybrid Fe3O4/SiO2/n-Si structures, Mater. Sci. Eng. B 211 (2016) 33–36.
[28] N.V. Volkov, A.S. Tarasov, E.V. Eremin, S.N. Varnakov, S.G. Ovchinnikov, S.M. Zharkov, Magnetic-field- and bias-sensitive conductivity of a hybrid Fe/SiO2/p-Si structure in planar geometry, J. Appl. Phys. 109 (2011) 123924.
[29] N.V. Volkov, E.V. Eremin, V.S. Tsikalov, G.S. Patrin, P.D. Kim, Y. Seong, D. Kim, N. Chau, Current-driven channel switching and colossal positive magnetoresistance in the manganitebased structure, J. Phys. D. Appl. Phys. 42 (2009) 065005.